Constant speed tip deflection determination using the instantaneous phase of blade tip timing data

D.H. Diamond*, P.S. Heyns and A.J. Oberholster

Centre for Asset Integrity Management, Department of Mechanical and Aeronautical Engineering, University of Pretoria, Pretoria 0002, South Africa

*Corresponding author. dawie.diamond@up.ac.za

Highlights

- Blade Tip Timing proximity probe signals are converted into the angular domain.
- Instantaneous phase information, using a quadrature filter, is used to calculate tip deflections.
- Experimental tests against other triggering criteria are performed.
- The proposed method demonstrates increased robustness against noise.

Abstract

Blade Tip Timing (BTT) is a non-intrusive measurement technique that can be used to estimate the vibration characteristics of rotor blades during turbomachine operation. BTT uses proximity probes mounted into the turbomachine casing to measure the Time-of-Arrival (ToA) of rotor blades at these proximity probes. The ToAs are determined using a triggering criterion on the proximity probe signal. Rotor blade tip displacements are then calculated from these ToAs. It is therefore imperative that the triggering criterion be as accurate as possible. This article proposes a new method to determine the tip displacement of rotor blades from a proximity probe signal. The method first converts the signal into the angular domain and then obtains the tip deflection through manipulation of the instantaneous phase in the signal. Three experimental tests are conducted where existing triggering criteria are compared to the proposed method. It is found that the proposed method is highly accurate in determining the tip deflections for a constant rotor speed.

Keywords: Blade Tip Timing; Triggering criteria; Quadrature filter

Nomenclature

$c(\theta)$	The result of convolving K_2 with $p(\theta)$
$\mathcal{F}$	Fourier transform
f	Frequency in the Fourier transform
g	Arbitrary time domain function
t_0	Time delay used to explain the Fourier shift theorem
G_2	The second derivative of a Gaussian.
H_2	The Hilbert transform of G_2
K_2	The quadrature filter used to expose the local phase information
$p(\theta)$	The proximity probe signal *after* it has been converted into the angular domain
R	Outside radius of the rotor blades[μm]
Δt	Difference between expected ToA and measured ToA [s]
δt	Error in ToA estimate [s]
x	Blade tip deflection [μm]
δx	Error in x due to incorrect ToA estimate [μm]

Greek Symbols

Λ	The mean absolute error between the reference result and the result from a noisy signal
θ	Angle [radians]
Ω	Rotor angular speed [radians/s]
$\phi(\theta)$	The phase of $c(\theta)$ [radians]
$\phi_0(\theta)$	The phase in the first revolution [radians]
θ_b	Angular location of blade number b [radians]

1. Introduction

Blade Tip Timing (BTT) is a non-intrusive method used to measure the vibration of rotor blades during operation [1], [2], [3], [4]. The method uses proximity probes mounted into the turbomachine casing around the rotor blade tips. A voltage pulse is generated by the probe each time a blade passes underneath it. This pulse is used to locate the Time-of-Arrival (ToA) of the blade at the probe.

In the absence of unsteady shaft speed or blade vibration, it is possible to predict these ToAs precisely. If, however, the blade tip is deflected due to vibration, the blade arrives at the proximity probe earlier or later than expected. This difference between the measured and expected ToA is used to calculate the tip deflection of the blade every time it passes the probe.

1.1. Determining rotor blade tip deflection

Rotor blade tip deflections are calculated from the ToAs. The tip deflections are then used to calculate BTT information such as blade resonant frequencies and amplitudes. The size of these amplitudes depends on the operating conditions. One source states that amplitudes vary between 100 µm during normal operation and 400 µm during blade resonance [5]. One commercial vendor claims that blade vibration amplitudes can range between 3 µm and 5 cm [6].

The accuracy of the BTT signals is correlated to the accuracy of the tip deflections. The vibration amplitude may be over- or underestimated, or missed completely, if the tip

deflections are not calculated accurately. Two conventional triggering criteria are now discussed, followed by two sources of noise that can corrupt the tip deflections.

1.2. Triggering criteria

Two of the most frequently used methods to calculate the ToAs are the *fixed voltage threshold* and the *constant fraction crossing* methods:

1. **Fixed voltage threshold:** The ToA is triggered by the signal crossing a fixed voltage threshold.
2. **Constant fraction crossing:** The ToA is triggered using a threshold on the downwards slope of the pulse. The threshold is a fraction of the pulse's amplitude and therefore changes according to the pulse's height.

These two methods are illustrated in Fig. 1 below.

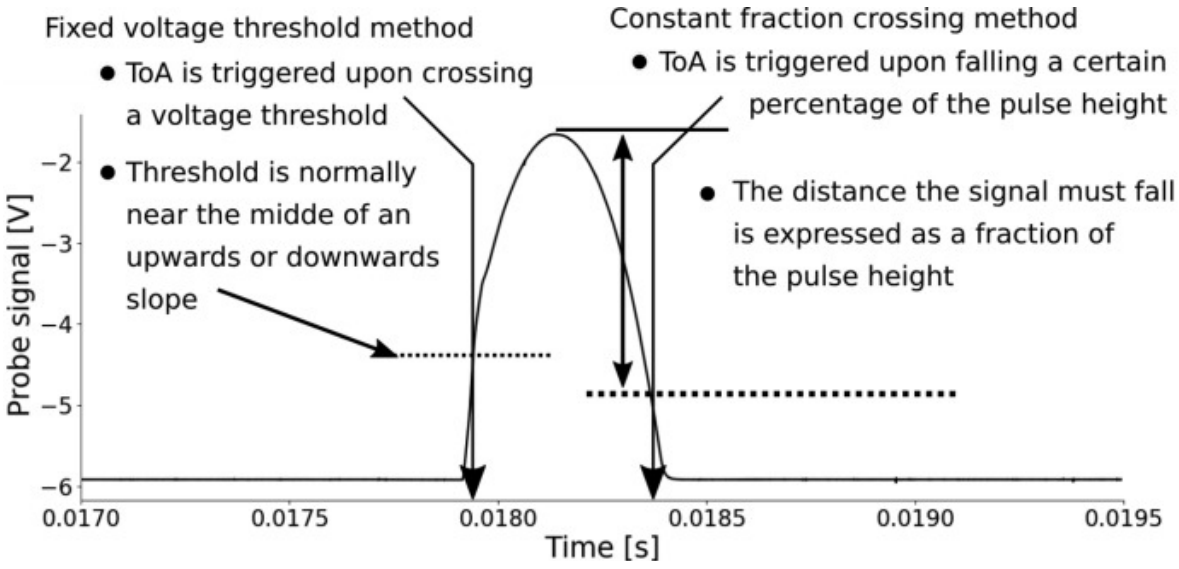

Fig. 1. Illustration of the two triggering criteria.

There are several sources of noise that can affect the accuracy of the triggering criteria. Such sources include shaft torsional vibration, proximity probe noise and a finite sampling rate. Two of these sources are now discussed in greater depth.

1.3. Proximity probe noise

There are two consequences of having noise in the proximity probe signal:

1. If noise is present on the rising or falling edge of a pulse near the triggering threshold, then the triggering will occur slightly earlier or later than it would have without the noise. This inaccuracy translates into a less accurate tip deflection.
2. It is possible for the noise level to be so severe that ToAs are incorrectly triggered. This can happen when the signal, due to noise, breaks through the threshold several times during a single pulse. Commercial software handles this problem by allowing

the user to specify a black-out window. The black-out window specifies the minimum amount of time that must pass between consecutive ToAs. There are other ways to deal with this as well, such as using one or two trigger levels to "arm" the BTT system and then taking the first ToA after the next threshold level has been crossed. All these methods are ways of choosing between multiple possible ToAs. The black-out window method selects the first ToA on a pulse and disregards the rest. There is no guarantee, however, that the first ToA is indeed the correct ToA. It is entirely possible for a wrong ToA to be measured, leading to incorrect tip deflections.

1.4. Effect of a finite sampling rate

The accuracy with which a BTT system can measure the ToAs is directly proportional to the data acquisition sampling rate. This statement is now illustrated using the conventional equation for tip deflection calculation [7], shown below.

$$x = \Omega \Delta\, tR \tag{1}$$

In Eq. 1 above, x indicates the rotor blade tip displacement, Ω indicates the rotor speed, R is the outside radius of the rotor blade and Δt is the difference between the measured ToA and the "expected" ToA in the absence of vibration. It is seen from Eq. 1 that the tip deflection is directly proportional to Δt and therefore the ToA. Even a very small error in the measured ToA can result in a large tip deflection error. The error in tip deflection per error in ToA is obtained by differentiating Eq. 1 and multiplying it with the error in the ToA, as done in Eq. 2 below.

$$\delta x = \Omega R \delta t \tag{2}$$

In Eq. 2, δt is the error in the measured ToA. Take, for instance, the simple example of a rotor operating at a constant speed of 3000 RPM with an outside diameter of 1 m. If the measured arrival time is incorrect by just 1 μs, the error in tip deflection is

$$\begin{aligned} \delta x &= \tfrac{3000 \times 2\pi}{60} \times 0.5 \times 10^{6} \times 1 \times 10^{-6} \\ \delta x &\approx 157\ \mu\mathrm{m} \end{aligned} \tag{3}$$

An error of 157 μm is non-negligible if the blade vibration is in the range of 100 μm–400 μm as suggested in [5]. Even a sampling rate of 100 MHz leads to an error of 1.57 μm, which can be large if one is investigating tip vibrations in the region of 5 μm [6].

1.5. Scope of this article

The triggering criteria already mentioned uses only one or two features of the pulse waveform, such as the first sample to cross a fixed voltage threshold. Most of the sampled waveform is therefore *not utilized* and effectively gets *thrown away*.

This article proposes a triggering criterion that uses the entire pulse shape, or at least a large amount of it. Our hypothesis is that because more of the pulse is used, the results will be less affected by noise. Two different analyses are conducted to test this hypothesis:

1. **Sensitivity to noise:** A test is conducted whereby the tip deflections are calculated on a noise-free signal. Increasingly severe noise is then added to the signal. The three triggering criteria are then used on the noisy signals and we measure the error between them and the noise-free results.
2. **Sensitivity to sampling rate:** A test is conducted whereby the tip deflections are calculated on a clean signal and at the highest possible sampling rate. The sampling rate of the signal is then progressively reduced, and the three triggering criteria are used to obtain the tip deflections. We then compare how closely the three methods can recover the noise free results.

The claims made in this article are limited to constant shaft speed cases.

2. Proposed method

Every BTT triggering criterion is used to calculate the delay of the pulse caused by the blade tip moving past the sensor. The delay in a time domain signal manifests itself as a phase shift in the frequency domain. This is called the Fourier shift theorem. Suppose we have a time-domain function *g(t)* and we impose a delay of t_0 on *g*. The Fourier shift theorem states that

$$\mathscr{F}\{g(t-t_0)\}(f) = e^{-j2\pi f t_0}\mathscr{F}\{g(t)\}(f) \tag{4}$$

Where $\mathscr{F}$ is the Fourier transform and *f* is frequency. Eq. 4 can be used to calculate the phase shift of each component in the frequency domain for a given delay in *g*. To illustrate this, consider a pure sinusoid with a frequency of 1 Hz and a time delay of 0.1 s:

$$g(t) = \sin(2\pi \times 1 \times t) \tag{5}$$

$$t_0 = 0.1\ s \tag{6}$$

We can calculate the phase shift caused by t_0 as follows:

$$e^{-j2\pi \times 1 \times 0.1} = e^{-0.62832j} \tag{7}$$

$$\left|e^{-0.62832j}\right| = 1 \tag{8}$$

$$\angle e^{-0.62832j} = -0.62832\ \text{radians} \tag{9}$$

A computational verification of this result is illustrated in Fig. 2 below.

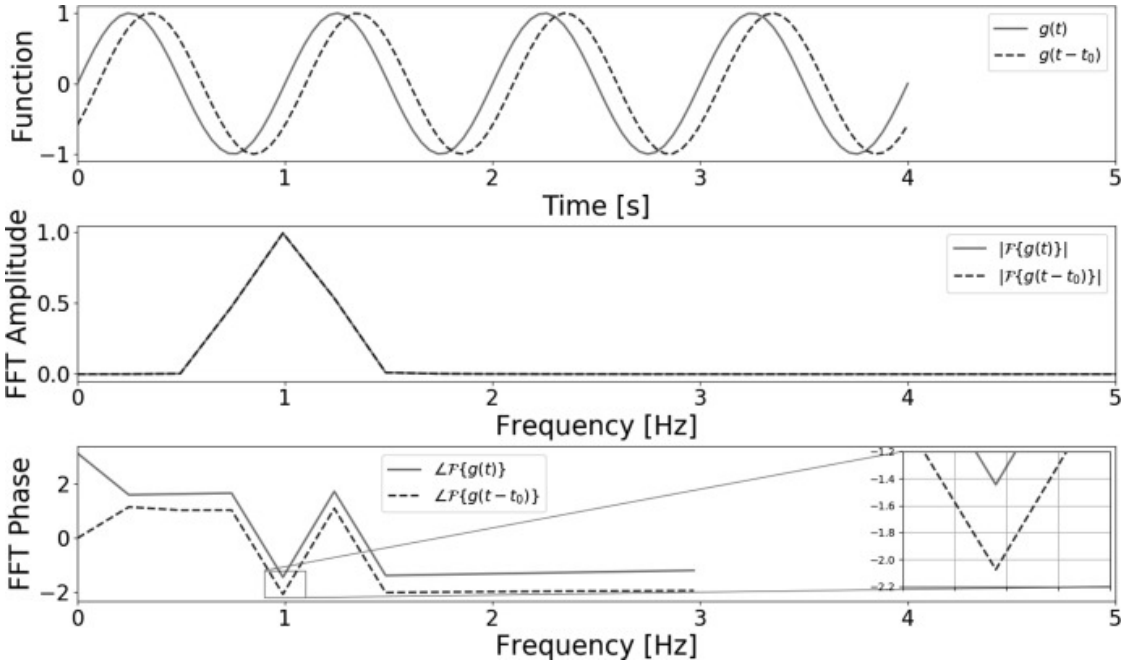

Fig. 2. A graphical illustration of the Fourier shift theorem for $g(t) = \sin(2\pi t)$ and $t_0 = 0.1$ s. πThe delay imposed on *g* creates a phase shift of −0.62832 radians.

Fig. 2 confirms the result from Eqs. (7), (9), i.e. that a phase shift of 0.62832 radians has taken place.

BTT signals are, however, more complex than this example. For one, BTT signals are nonstationary, meaning each pulse will have a different time delay and consequently a different phase shift. Also, BTT pulses do not result in a single frequency when transformed into the frequency domain. They result in broadband spectra. These difficulties have been effectively dealt with in Motion Magnification (MM) literature [8], [9], [10], [11]. In MM, small changes in an image's position is found by extracting and manipulating the *instantaneous phase* at every location in an image. The instantaneous phase of a signal can be obtained by convolving that signal with a *quadrature filter*. The proposed method follows a similar approach to that used in MM. The proposed method is broken down into three steps:

Step 1: Convert the proximity probe signal into the angular domain. The shaft encoder is used to express the proximity probe signal in the angular domain. In other words, the proximity probe signal is no longer expressed in terms of time. The signal captured by the proximity probe starts at 0 radians and ends at 2πradians for each shaft revolution. This is done to remove delays in the proximity probe signal that can be attributed to differences in shaft speed instead of a vibrating blade. This step is necessary to cater for small variations in shaft speed.

Step 2: Apply a quadrature filter. A complex filter is convolved with the proximity probe signal. The purpose of this convolution is to expose the *instantaneous phase* at each pulse.

Step 3: Convert instantaneous phase into tip deflection. The instantaneous phase is converted into a delay for each pulse. Because the proximity probe signal is expressed

in the angular domain, the delay is in units of radians. The delay is then multiplied with the blade's length to obtain the tip deflection.

The three steps are now discussed in turn.

2.1. Conversion of the proximity probe signal into the angular domain

Conversion of the proximity probe signal into the angular domain is simple. Many methods of doing this exist [12], [13]. For the purposes of this article, Eq. 10 is used.

$$\theta\left(t\right) = \frac{2\pi}{t_{\text{end}} - t_{\text{start}}}\left(t - t_{\text{start}}\right) \tag{10}$$

In Eq. 10, t_{start} and t_{end} refer to the start and end of a revolution as determined using the tachometer.

Fig. 3 illustrates the effect this has on the proximity probe signal. There are five blades on the test rotor used for Fig. 3. A single proximity probe was used to measure for three consecutive revolutions. The three signals are shown in Fig. 3a) and b). A zoomed-in portion of a) is shown in b). Fig. 3c) and d) show the same signals as in a) and b), only after they have been converted to the angular domain. It can clearly be seen that the pulses in the angular domain are closer to one another than the pulses in the time domain. It is important to note that we are not changing the signal in any sense, it is merely represented in a different domain. In fact, all BTT triggering criteria perform conversion into the angular domain. To demonstrate this point, Eq. 11 rewrites the standard way to convert from time delay to tip deflection such that the conversion to the angular domain is apparent.

$$\frac{\delta x}{R} = \overbrace{\Omega \Delta t}^{\text{Conversion to angular domain}} \tag{11}$$

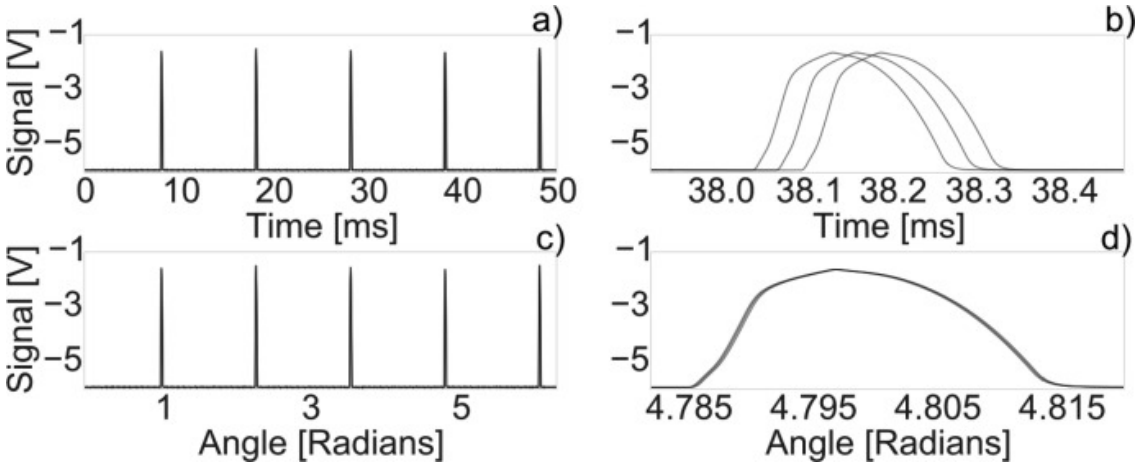

Fig. 3. Proximity probe signals from three consecutive revolutions superimposed over one another. a) All three revolutions superimposed over one another in the time domain. The revolutions have been aligned to start at $t = 0$. b) The same signals as in a) only zoomed into a single pulse, c) the proximity probe signals superimposed in the angular domain, i.e. the proximity probe signals as a function of shaft circumferential position, d) the same signal as in c) only zoomed into a single pulse.

The first, second and third revolutions are not individually marked as it does not matter for the purposes of this discussion and only clutters up the image.

The proximity probe signal that has been converted into the angular domain will henceforth be referred to as $p(\theta)$.

2.2. Apply a quadrature filter

As stated earlier in the article, a quadrature filter is used to expose the local phase in the signal. The intuition behind this has been given earlier using the Fourier shift theorem. More in-depth theory about the use of quadrature filters is outside the scope of this article. Readers are referred to original MM and instantaneous phase literature for a deeper understanding [14], [15], [16], [17], [18]. The quadrature filter used for the proposed method is the analytic signal of the second derivative of a Gaussian. This filter has been used to great effect in other applications [9], [19]. The filter is denoted by K_2 and is given in Eqs. (12), (13), (14).

$$K_2(\theta) = G_2(\theta) + iH_2(\theta) \tag{12}$$

$$G_2\left(\theta\right) = e^{-\frac{\theta^2}{\rho^2}}\left(\frac{1}{\rho^2} - 2\frac{\theta^2}{\rho^4}\right) \tag{13}$$

$$H_2\left(\theta\right) = \frac{1}{\pi}P\int_{-\infty}^{\infty}\frac{G_2(\tau)}{\theta-\tau}d\tau \tag{14}$$

In Eq. 12, $K_2(\theta)$ is the sum of $G_2(\theta)$ and its Hilbert transform, $H_2(\theta)$. $G_2(\theta)$ is the second derivative of a Gaussian function with variance ρ^2 as shown in Eq. 13. $H_2(\theta)$ is given in Eq. 14 [20]. The Hilbert transform of a Gaussian, or derivatives of a Gaussian, does not have a closed form solution [21] and must be calculated computationally. Most scientific packages have built-in functions to compute the Hilbert transform. The Python function scipy.signal.hilbert was used for this article. To illustrate the filter, four different values for the scaling parameter, or ρ, are used and the resulting quadrature filters are plotted in Fig. 4. The four values for the scaling parameter, ρ, are 0.05, 0.1, 0.15, and 0.20 radians respectively.

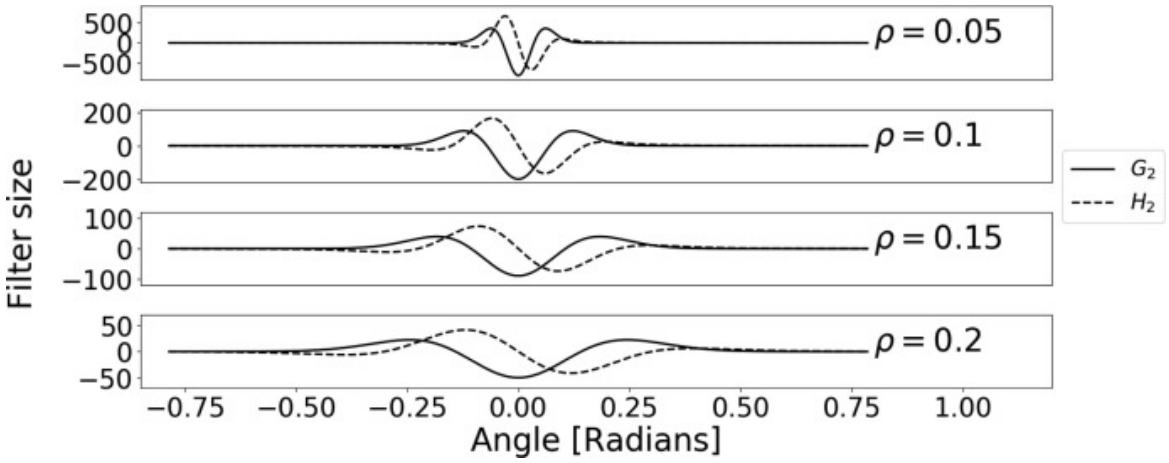

Fig. 4. The complex filter used for the proposed method. Four different filters are shown for illustrative purposes, the four filters have different scaling parameters of 0.05, 0.1, 0.15, and 0.2 radians respectively.

The quadrature filter is now convolved with the proximity probe signal. If a real-valued function is convolved with a quadrature filter, the response contains real and imaginary components. Eq. 15 shows this convolution.

$$c(\theta) = p(\theta) * K_2(\theta) \tag{15}$$

In Eq. 15, $p(\theta)$is a symbol used to denote the proximity probe signal after it has been expressed in the angular domain and * is the linear convolution operator. The result of the convolution is denoted by $c(\theta)$. To illustrate $c(\theta)$, a full convolution is performed between $K_2(\theta)$ and $p(\theta)$, and the result is shown in Fig. 5.

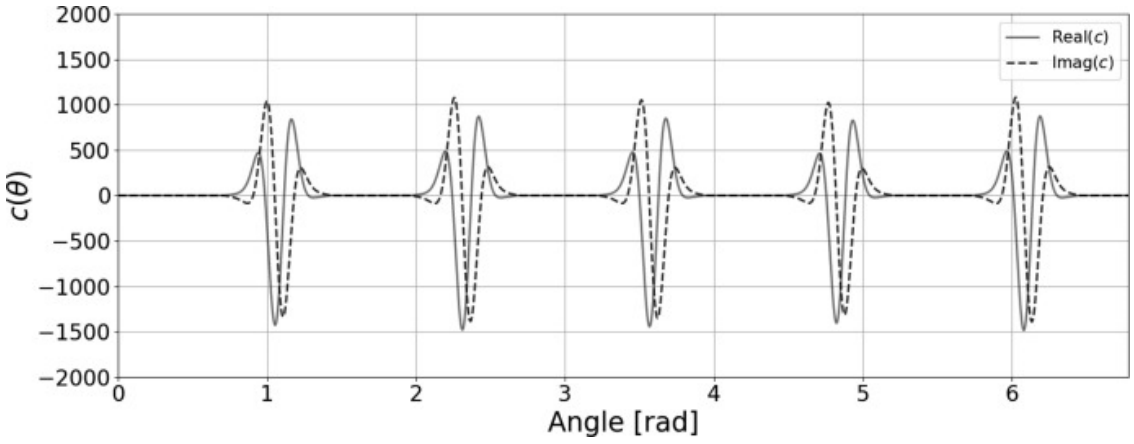

Fig. 5. This figure illustrates the result of convolving the proximity probe signal with $K_2(\theta)$. The scaling parameter was $\rho = 0.09$ for this illustration.

Now, finally, the phase is obtained from $c(\theta)$ by expressing it in polar form, as shown in Eq. 16.

$$\phi(\theta) = \angle c(\theta) \tag{16}$$

We do not create a new function for the *amplitude* of $c(\theta)$ because the amplitude is not used in the proposed method. The phase, $\phi(\theta)$, for the signal in Fig. 5 can be seen in Fig. 6.

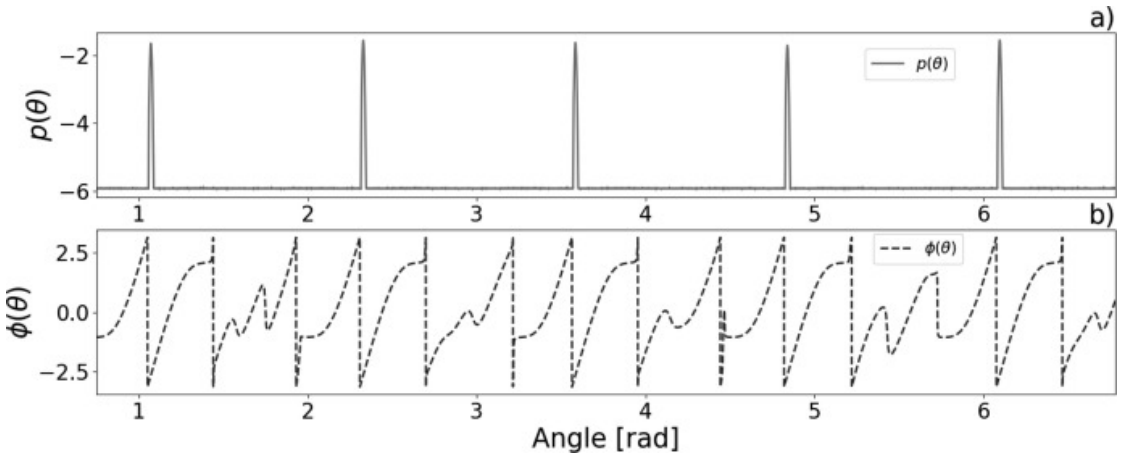

Fig. 6. Illustration of $\phi(\theta)$ derived from the signal in Fig. 5.

2.3. Convert instantaneous phase into tip deflection

Now for the final step. The instantaneous phase is converted into a tip deflection using Eq. 17.

$$x\left(\theta\right) = Rd\,\theta\left(\frac{\phi(\theta)-\phi_0(\theta)}{\phi(\theta)-\phi(\theta-d\theta)}\right) \tag{17}$$

In Eq. 17, *x* is the tip deflection and $\phi_0(\theta)$ is the phase signal from the first revolution. The first revolution therefore serves as a reference for the other values. Eq. 17 has been taken straight from MM literature [9], [11], [15], [19]. The quantity is the quantity that governs the sample spacing of the quadrature filter. This value should be as small as the smallest sample spacing found in $p(\theta)$.

A full convolution of $p(\theta)$ with $K_2(\theta)$, as shown in Fig. 5, is not necessary. We only need to apply Eq. 17 once at every pulse location to get a tip deflection for every blade. The angular location used to apply Eq. 17 at for blade number *b* is denoted by θ_b. To determine θ_b, a threshold value is used on the rising and falling flanks of the reference signal (i.e. the signal obtained from the first revolution). The θ_b values are taken to be in the middle of these two angular positions. See Fig. 7 for an illustration. Note that, when performing the convolution, $p(\theta)$ is interpolated to have the same spacing as $K_2(\theta)$. This ensures the two signals are aligned exactly. Simple linear interpolation is used in this article.

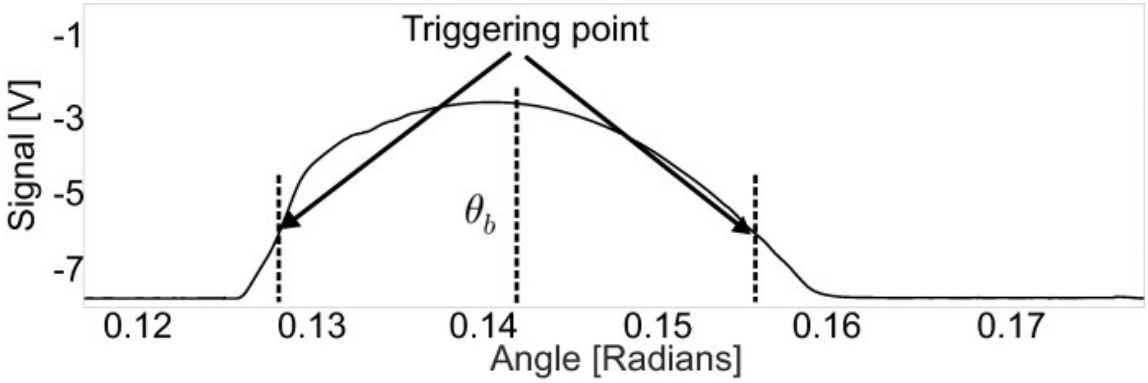

Fig. 7. Determination of the angular location, θ_b, where the instantaneous phase of each blade *b* is determined. It is located halfway between the rising and falling edges of the pulse.

3. Experimental setup and method

3.1. Experimental setup

The turbomachine used for the experiment consists of a shaft supported by two bearings, driven by a three phase motor. The shaft encoder consists of a zebra tape and an optical probe. This produces TTL pulses as the output signal. The shaft encoder has 78 sections but only every 78th revolution was used for the experiments, rendering the encoder a Once Per Revolution (OPR) encoder. The rotor, a blisk with five rectangular blades, has an outside diameter of 324 mm and is end-mounted onto the shaft with a taper-lock fastening mechanism. A single eddy-current probe was used for the experiment. The probe used in this experiment has a sensitivity of 8 mV/μm and a measuring range of 2 mm. The data acquisition system is a NI USB-6366 system, capable of sampling and logging analogue signals at a maximum rate of 2 MHz. LabView was used to control the data acquisition system. Fig. 8a) shows a front view of the rotor and b) shows the shaft encoder.

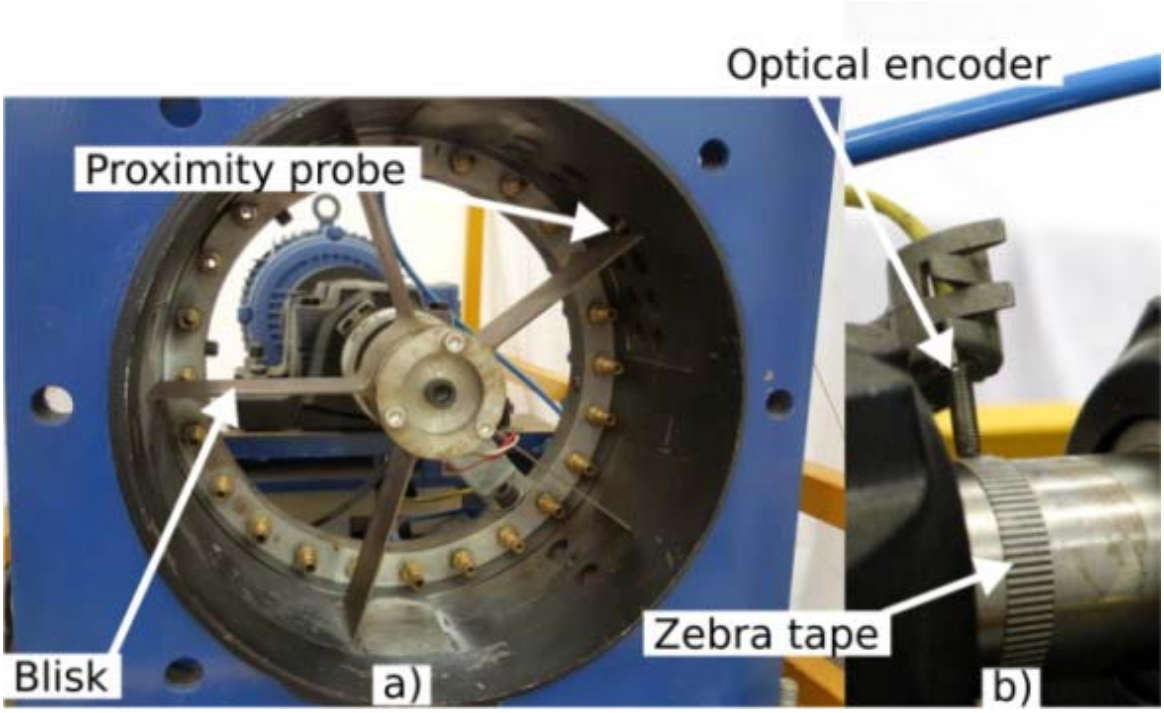

Fig. 8. Illustration of experimental setup. a) an axial view of the turbomachine with the blisk and an eddy current probe indicated, b) the optical sensor and the zebra tape on the shaft.

3.2. Experimental method

It is hypothesised that the newly proposed method is more accurate than conventional trigger-based methods. The reason for this is because the proposed method uses a larger portion of the pulse to determine the pulse shift than conventional methods. This hypothesis needs to be supported by experimental results.

The ideal way to prove this would be to compare the triggering criteria results to the results from another, independent, method. The independent method must, by definition, be more accurate and reliable than the triggering criterion. It is unfortunate that such a method does not exist in BTT. Some attempts at alternative methods have, however, been made. One may attempt to use strain gauges along with some kind of calibration test to correlate strain to tip deflections. This approach simply does not yield reliable enough results for to validate the size of tip deflections [7], [22], [25] but can be used to validate vibration frequencies. Another option is to use a digital camera to capture the blade tip as it moves past the location of the probe. This method was used by [23]. In this approach, Perspex panels, with marked grid lines used to measure distance, were installed into the rotor's casing above the blades. A digital camera was placed above the Perspex panels, looking down onto the blade tip chord. A strobe light was synchronised to the tachometer, and photographs of a blade's position were taken over many revolutions. A comparison between the camera results and the BTT results showed good general agreement between the two methods. The method was, however, not used for quantitative comparison of every tip deflection measurement. Even if it is possible to compare individual tip deflection measurements with camera-measured results, the accuracy of the camera-based method itself would also have to be validated. BTT and Laser Doppler Vibrometry (LDV) have also been compared in [24] for out of plane

vibrations. It was found that both methods could be used to measure sinusoidal vibration, but the sizes of the tip deflections from the two methods were not close to one another.

Instead of using an independent measurement, we are going to *gradually increase the noise* in the proximity probe signal and then measure each criterion's performance on the noisy signal. It stands to reason that a triggering criterion's performance will deteriorate as the noise increases. The triggering criterion that most closely reproduces the original noise-free tip deflections is therefore the most accurate criterion. The metric used to evaluate the accuracy of each increasing level of noise to the original noise-free result is given in Eq. 18.

$$\Delta = \frac{\sum_{m=1}^{M} \sum_{b=1}^{5} \left| x_{\text{ref}}\left(\theta_b\right) - x\left(\theta_b\right) \right|}{5M} \tag{18}$$

In Eq. 18, Δ is the mean absolute error between all the tip deflections in a test compared to the noise-free reference for that triggering criterion. The number of revolutions in the analysis is denoted by M and b represents the blade index. There are five blades in the rotor. Note that the blades are vibrating because of the ambient air excitation.

Given this metric and approach, five tests are performed. The five tests and their methods are listed below:

- **Test 1: Noise free test.** In this test, the reference results for the three triggering criteria are determined. The rotor is run at three different shaft speeds; 600, 900, and 1200 RPM. The analogue signals are then measured for 10 s at a rate of 2 MHz. The tip deflections for all blades are calculated using the proposed method, the fixed voltage threshold method, and the constant fraction crossing method. The results from the three tests are compared to one another as a sanity check to ensure they produce approximately the same tip deflections and have therefore been implemented correctly. The scaling parameter, ρ, for Tests 1, 2 and 3 is 0.012 radians. Test 4 shows why this value is used.
- **Test 2: Increasing Gaussian noise.** Gaussian noise with a mean of zero is added to the reference signals measured in Test 1. Ten different levels of Gaussian noise are added. The standard deviations of the levels are 0.01, 0.02, 0.03, 0.05, 0.1, 0.2, 0.3, 0.4, 0.5 and, 0.6 V. At each noise level, the triggering criteria are used to obtain the tip deflections and each criterion is compared to its own reference from Test 1. Eq. 18 is then used to determine the accuracies of the three triggering criteria. Testing for other kinds of noise falls outside the scope of this article.
- **Test 3: Decreasing sampling rate.** The sampling rate of the reference signals are reduced in 20 different levels and the accuracies of the three triggering criteria are determined at each level. Sampling rate reductions, or decimation, are performed in the following degrees: 2, 3, 4, 5, 6, 7, 8, 9, 10, 20, 30, 40, 50, 60, 70, 80, 90, 100, 110, and 120 times. In other words, the resulting sampling rates for the 20 levels are 1 MHz, 666.67 kHz, 500.0 kHz, 400.0 kHz, 333.33 kHz, 285.71 kHz, 250.0 kHz, 222.22 kHz, 200.0 kHz, 100.0 kHz, 66.67 kHz, 50.0 kHz, 40.0 kHz, 33.33 kHz, 28.57 kHz, 25.0 kHz, 22.22 kHz, 20.0 kHz, 18.18 kHz, and 16.67 kHz.
- **Test 4: Sensitivity to ρ.** The proposed method depends on the choice of ρ. The same methodology as used in Test 2 and Test 3 can be used to determine an adequate value for ρ. Test 2 and Test 3 is therefore repeated for the proposed method only and ρ is varied between 0.005 radians to 0.05 radians. It becomes clear that this analysis can be used to determine a reasonable value for ρ.

- **Test 5: Computational comparison.** The computational time of the three methods are compared against one another for the implementation used in this article.

4. Results and discussion

The shaft speed profiles from the three measurements are shown in Fig. 9. We do this to demonstrate to the reader that, although the claims made in this paper are limited to constant speed cases, the speed does in fact vary. It is seen from Fig. 9 that all three shaft speed profiles, though almost constant, varies approximately 1 RPM above and below their intended values. The results presented in this article are therefore valid where small speed fluctuations are present.

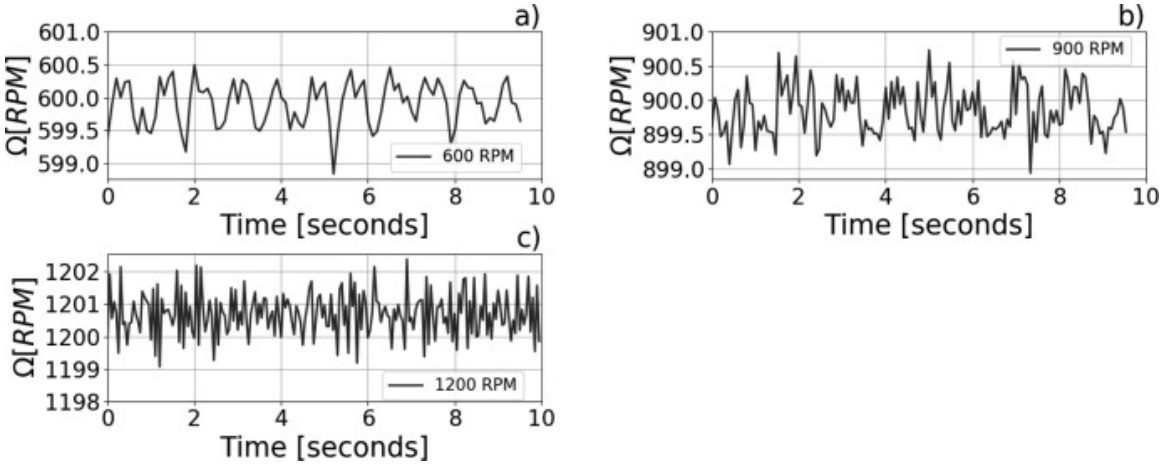

Fig. 9. Shaft speed variations for the a) 600 RPM b) 900 RPM and c) 1200 RPM measurements.

The parameters for the three triggering criteria are:

- **Phase based method:** The scaling parameter, ρ, is chosen as 0.012 radians. The filter width is 8ρ and it is made up of 1601 equidistant samples in the angular domain.
- **Fixed voltage threshold method:** The threshold for the fixed voltage threshold method is −4.7 V on the rising edge of the pulse. This value results in the most accurate answers for the fixed voltage threshold method.
- **Constant fraction crossing method:** The constant fraction crossing method is triggered at a 50 % fall from the maximum of each pulse.

4.1. Test 1: Noise free test

The tip deflections for all three shaft speeds are calculated using the three triggering criteria. The results are used throughout Test 2 and Test 3 as the reference results. To give the reader an idea of the tip deflection size for these experiments, the blade 1 tip deflections over the first 5 revolutions for each triggering criterion is given in Table 1.

Table 1. Table showing the tip deflections of the first blade over the first 5 revolutions. It is seen that the tip deflections from the different triggering criteria are close to one another.

Revolution	Phase based	Fixed voltage threshold	Constant fraction crossing
1	−108.044738	−107.185851	−105.601921
2	30.483787	26.368992	35.364730
3	80.057773	79.727256	81.249474
4	−42.354994	−41.468956	−42.103858
5	103.148690	102.873084	101.785767

It is important to establish that the three triggering criteria produce approximately the same results under noise-free conditions. We can plot the tip deflections from all three methods against one another and perform a linear fit between them. The results should yield an

value close to one. This is illustrated in Fig. 10.

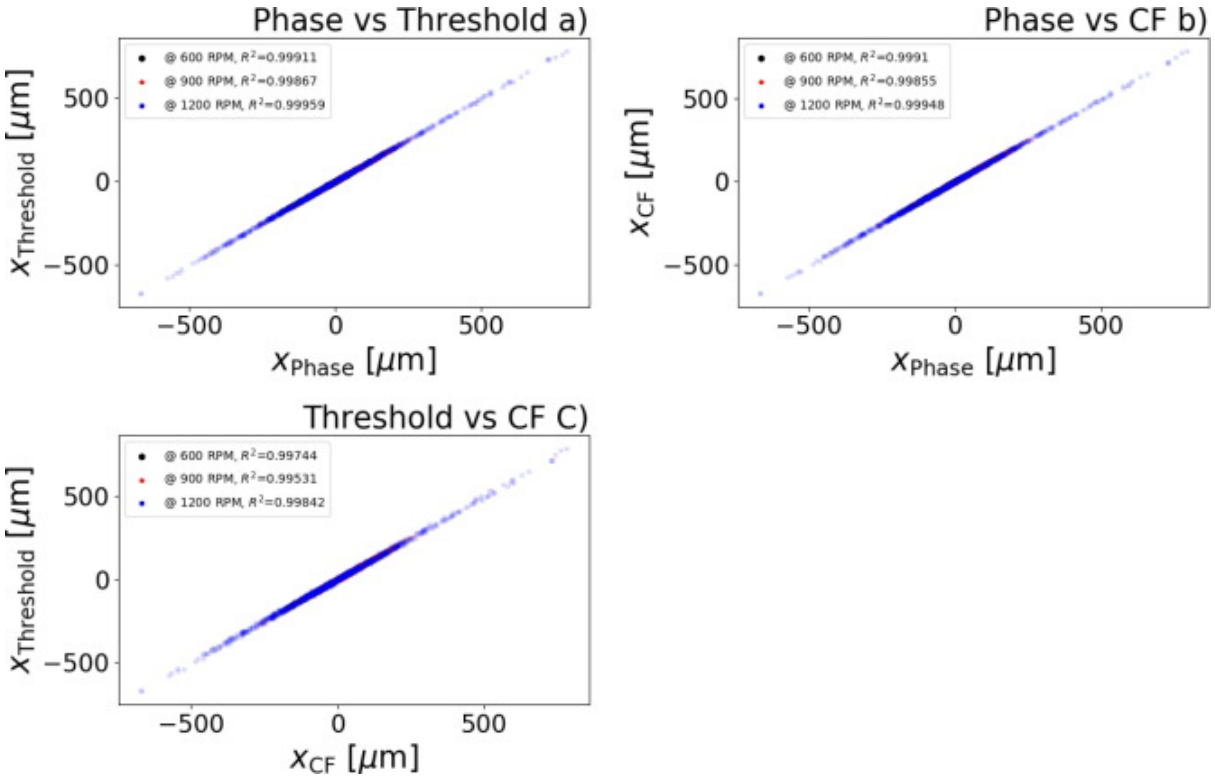

Fig. 10. A scatterplot of the tip deflections from different triggering criteria plotted against one another. This plot is for the reference test case, i.e. the noise-free case.

In Fig. 10, the tip deflections from the different triggering criteria for the noise-free case are plotted against one another. In Fig. 10 a), the phase based approach is compared to the fixed voltage threshold method. Since the tip deflections from the two criteria are so close to one another, it is difficult to discern the results for different shaft speeds. The 1200 RPM case was plotted last and as such appears on top. It is clearly seen that the tip deflections from the two methods are very close to one another. The R^2 values for the 600, 900, and 1200 RPM measurements are 0.99911, 0.99867, and 0.99959 respectively. Similar R^2 values are found in Fig. 10b) where the phase based method is compared to the constant fraction crossing (CF) method and in Fig. 10c) for the CF method vs the fixed voltage threshold method. These

results confirm that the triggering criteria have been implemented correctly and perform very *well in the absence of noise.*

4.2. Test 2: increasing Gaussian noise

The reference results have been obtained. Now we present the performance of the three triggering criteria when subjected to increasing levels of noise. As mentioned earlier, zero-mean Gaussian noise is added in 10 different levels. The standard deviations (std) of the added noise are 0.01, 0.02, 0.03, 0.05, 0.1, 0.2, 0.3, 0.4, 0.5, and 0.6 V. Fig. 11 shows the results of this test. It is clear from Fig. 11 that the phase based method performs more accurately than the constant fraction crossing and fixed voltage threshold methods throughout all levels of noise and all shaft speeds. Our hypothesis concerning the proposed method's accuracy as it pertains to Gaussian noise is therefore confirmed. Even under the most severe noise of 0.6 V, the phase based approach is, on average, only 20 μm less accurate than the noise-free case. This compares favourably to the other two methods, where an average error of between 200–1000 μm appears for the same noise level. To get a sense of how much noise 0.6 V is, Fig. 12 plots a noise-free pulse along with the same pulse that has been corrupted by 0.6 V Gaussian noise. It is seen in Fig. 12 that a lot of noise is present in the pulse. The fixed threshold of −4.7 V is crossed many times. A black-out window the length of the pulse was used to stop multiple triggers from the fixed voltage threshold method.

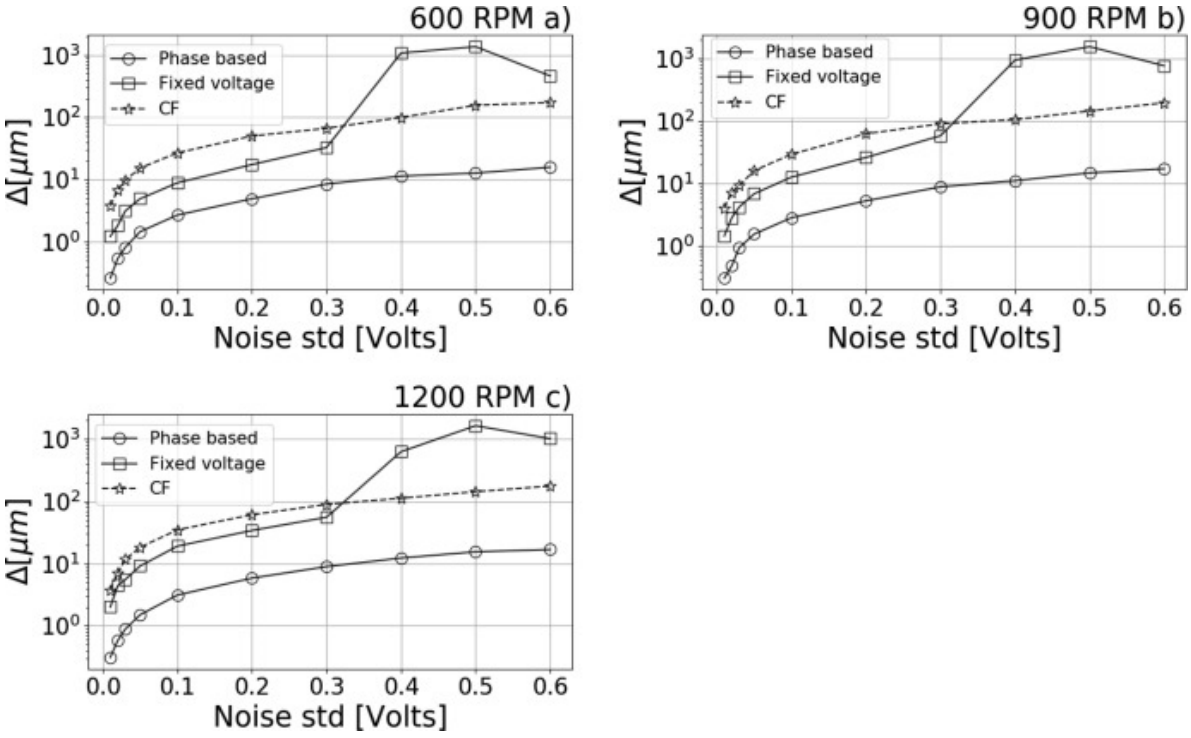

Fig. 11. Test case 2 results where zero-mean Gaussian noise is added in 10 different levels to test the robustness of the triggering criteria to noise. a) The results for the measurement at 600 RPM, b) the results for the measurement at 900 RPM and c) the results for the measurement at 1200 RPM.

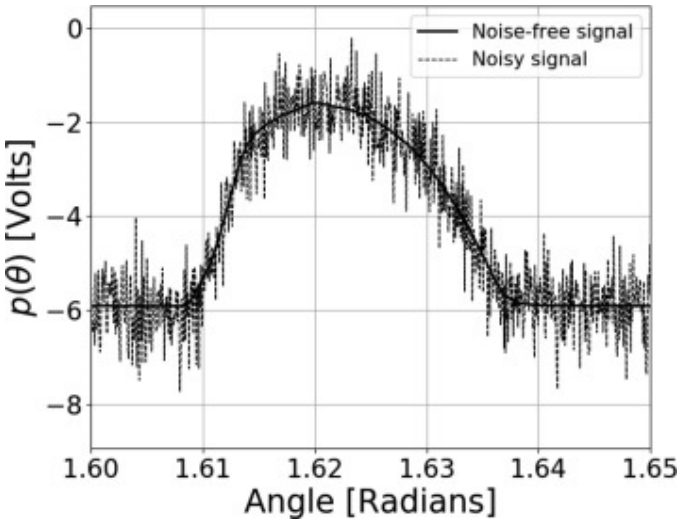

Fig. 12. A single pulse from the 1200 RPM measurement. The pulse is shown without any additional noise using a solid black line. The same pulse that has been corrupted with 0.6 V standard deviation Gaussian noise is shown using a dotted line.

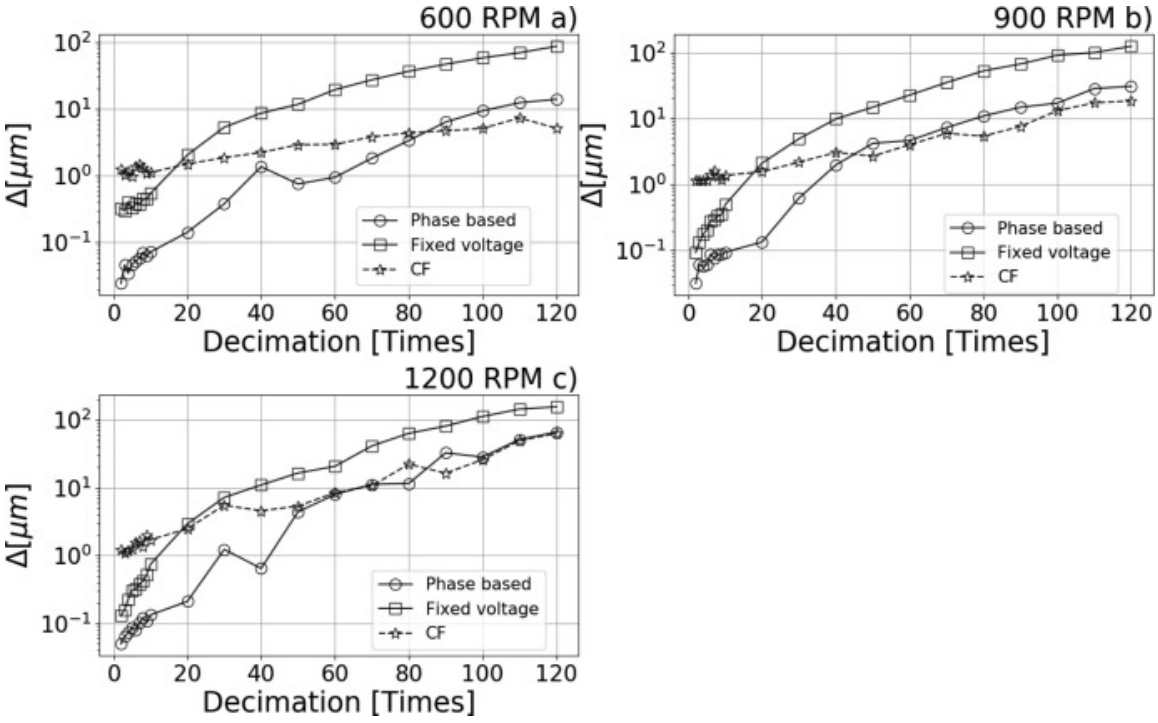

Fig. 13. The three figures show how the triggering criteria perform when the proximity probe signal's sampling rate is reduced several times. a) The average mean error of the three triggering criteria for the 600 RPM measurement, b) the results for the 900 RPM measurement and c) the results for the 1200 RPM measurement.

4.3. Test 3: decreasing sampling rate

As stated earlier, a decrease in the sampling rate should generally result in less accurate tip deflections. For this test, the reference signals are *decimated*, (i.e. their sampling rates decreased) using progressively more severe reductions. The following 20 levels of decimation are used: 2, 3, 4, 5, 6, 7, 8, 9, 10, 20, 30, 40, 50, 60, 70, 80, 90, 100, 110, and 120 times. In other words, if the decimation level is 10, then only every 10th sample from the original signal is retained. These levels of decimation result in the following sampling rates: 1 MHz, 666.67 kHz, 500.0 kHz, 400.0 kHz, 333.33 kHz, 285.71 kHz, 250.0 kHz, 222.22 kHz, 200.0 kHz, 100.0 kHz, 66.67 kHz, 50.0 kHz, 40.0 kHz, 33.33 kHz, 28.57 kHz, 25.0 kHz, 22.22 kHz, 20.0 kHz, 18.18 kHz, and 16.67 kHz. The results are shown in Fig. 13.

It is seen from Fig. 13 that the phase based method performs more accurately than the fixed voltage threshold method in all cases. The phase based method performs better than the constant fraction crossing method initially, but for all three shaft speeds there are points at which the constant fraction crossing method becomes more accurate than the phase based approach.

The reason this happens can be explained by showing a pulse where the sampling rate has been reduced 100 times. This pulse is shown in Fig. 14.

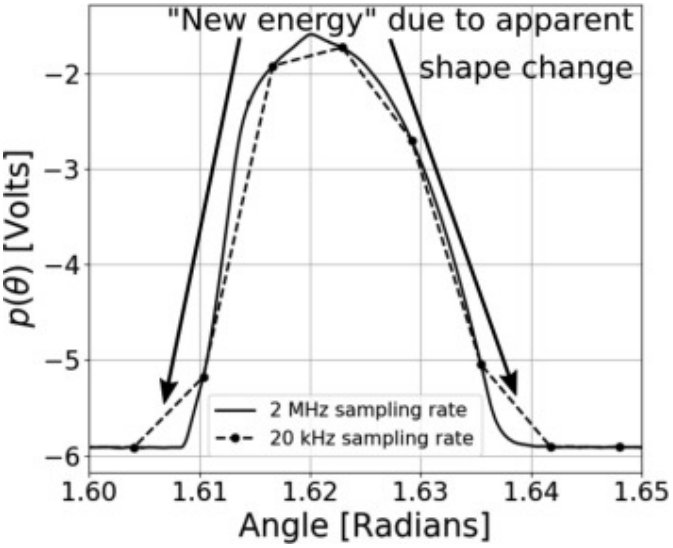

Fig. 14. A single pulse from the 1200 RPM measurement is shown.

In Fig. 14, a single pulse sampled at two different sampling rates is shown. The original pulse sampled at 2 MHz is shown using a solid line. The pulse after decimation by a factor of 100 is shown by a dotted line with circular markers. The sampling rate of this decimated pulse is therefore 20 kHz. It is seen that the 20 kHz pulse has a different apparent shape than the 2 MHz pulse. The 20 kHz pulse appears to have raised edges. The phase based method therefore finds energy next to the pulse where no energy is present in the reference signal. The phase based method does not perform as well where the pulse *shape* changes, only when the pulse position changes and the shape remains approximately constant.

It is of course true that *any reduction* in sampling rate does change the pulse shape. The performance of the phase based method is not affected by small changes in pulse shape. Large shape changes and significant apparent new energy needs to be present before the performance starts to deteriorate. The smallest decimation factor where the phase based method becomes less accurate than the constant fraction crossing method is 45 (i.e. at a sampling rate of 44.4 kHz) in the 900 RPM measurement. It is worth mentioning that this is an extremely low sampling rate for BTT. Most laboratories can easily manage 100 kHz and above.

It also appears in all three figures that the error of the phase based approach stabilises after a decimation rate of 100. We do not believe this is the case. We believe this is rather because of the using a log scale to show the results.

The hypothesis that the proposed method performs more accurately than the other two methods is therefore confirmed given the limitation that the pulse shape must be captured relatively accurately. The precise definition of when a pulse is captured properly lies outside the scope of this article.

It must be noted here that the sampling rate of the tachometer is never reduced.

4.4. Test 4: sensitivity to

Fig. 15 below shows the sensitivity of the proposed method to the choice of ρ if varying levels of white noise are added to the reference signals. Three levels of noise are added with the following standard deviation (std) values: 0.01, 0.1, and 0.5 V.

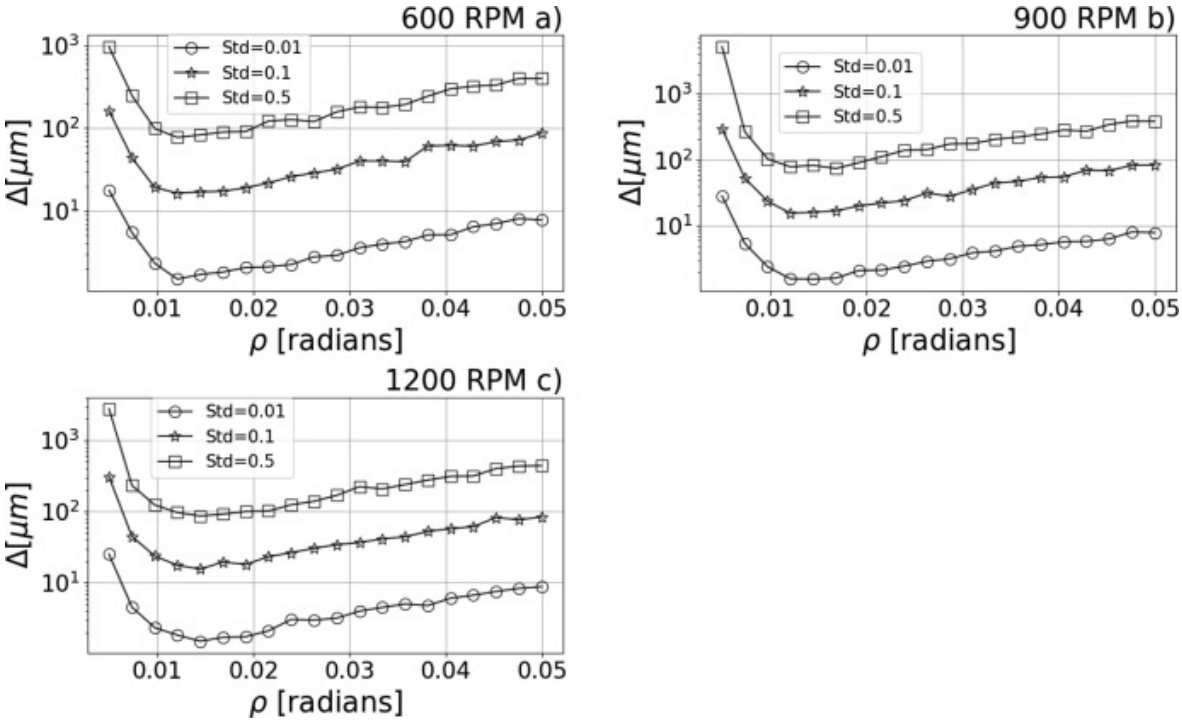

Fig. 15. This figure shows the sensitivity of the proposed method to the scaling parameter ρ for the a) 600 RPM, b) 900 RPM and 1200 RPM case.

It is seen from Fig. 15 that all the results have the same trend. At $\rho = 0.005$ all the analyses results in large errors. The accuracy of the phase based method increases as ρ enters the 0.012–0.02 range. The value for ρ that most often results in the most accurate answer is 0.012 radians. The scale in Fig. 15 is a log scale. When considering this, it seems that choosing any value between 0.012 and 0.02 is sensible.

We now present, in Fig. 16, the sensitivity of the phase based method to ρ as the sampling rate is reduced. Three different levels of decimation are performed, the sampling rate is reduced 2, 10, and 50 times; resulting in sampling rates of 1 MHz, 200 kHz and 40 kHz.

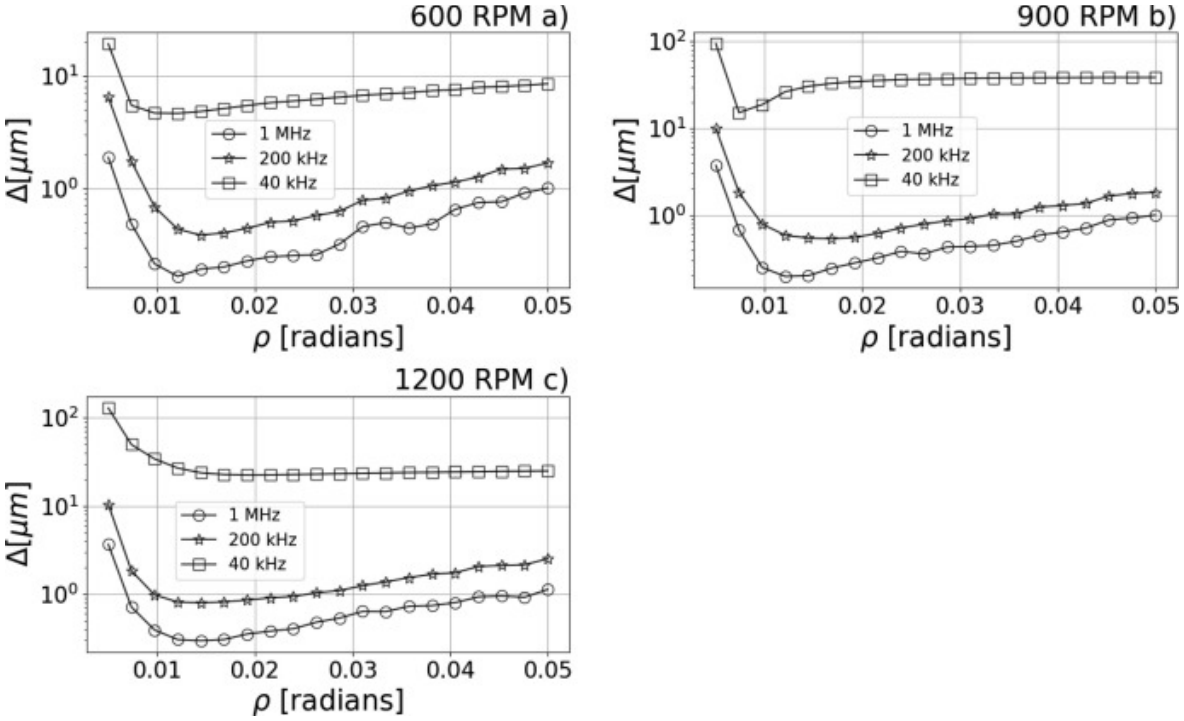

Fig. 16. This figure shows the proposed method's sensitivity to reductions in sampling rate for a) 600 RPM, b) 900 RPM and c) 1200 RPM.

Similar trends are observed in Fig. 16 as those in Fig. 15. It is seen that, for most of the analyses, a $\rho = 0.012$–0.02 yields the most accurate answers. The exception to this is for a sampling rate of 40 kHz at 600 RPM and 900 RPM. In these analyses, the optimal ρ value is smaller than $\rho = 0.012$. This makes sense, a smaller ρ leads to the phase based method using less of the pulse and therefore "seeing" less of the apparent pulse shape change. The 40 kHz analysis for the 1200 RPM case does not seem to have a well defined minimum, rather an asymptote. Of all the analyses done here, the combination of a 40 kHz sampling rate and a shaft speed of 1200 RPM results in the least samples over the pulses. We believe the phase based method simply cannot deal with this shape change, resulting in higher inaccuracies than obtained using the optimal ρ values for 600 RPM and 900 RPM.

The approach taken in this section can be taken for any other combination of probe and blade tip. One can take the original signal and add increasing levels of noise to find an adequate value for ρ. This is why a value of ρ radians was chosen for tests 1, 2 and 3.

4.5. Test 5: computational time analysis

A comparison of the computational time required to perform the reference analyses is now shown. The computation for each shaft speed is performed 20 times and the average over the 20 times is reported in Fig. 17.

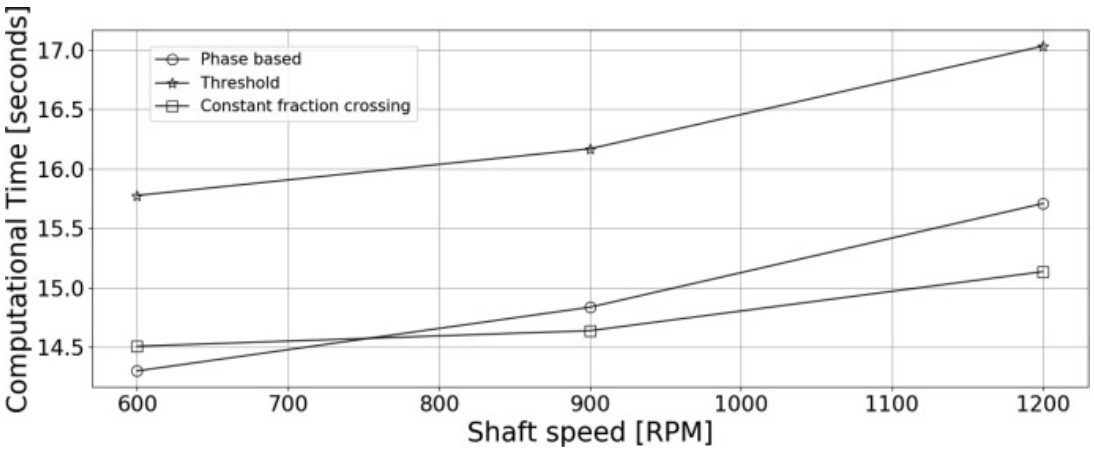

Fig. 17. The average computation time required to perform 20 analyses at each shaft speed for every triggering criterion.

In Fig. 17 it is seen that 14–17 s are required to process 10 s' worth of BTT data. The fixed voltage threshold method is the most expensive. The reason for this is because of the black-out window that was implemented to prevent multiple triggering of ToAs. The phase based method and the constant fraction crossing method runs for close to the same computational times, though it seems as if the phase based approach becomes more expensive as the shaft speed increases. This makes sense because a higher shaft speed results in more pulses that needs to be convolved with the quadrature filter. Convolution is more expensive than determining a trigger. Nonetheless, no method can be considered prohibitively expensive when compared to the other methods. Note that the code used for this analysis is not optimised for maximum speed. It is written for maximum readability as the code is open source and can be found at https://github.com/dawiediamond/pyphasetoa.

5. Conclusion and limitations

This article presented a new method to determine the tip deflections of rotor blades from BTT data. The method has three steps. Firstly, the proximity probe signal is expressed in the angular domain instead of the time domain. Secondly, a quadrature filter is used to expose the instantaneous phase of each pulse and, finally, the instantaneous phase is converted into a tip deflection.

Experiments are conducted at three different shaft speeds, i.e. 600, 900, and 1200 RPM. In the experiments, the proposed method is compared to the constant fraction crossing and fixed voltage threshold methods. All three triggering criteria are first used to determine the tip deflections in the absense of noise. These results serve as the reference results. Two tests are then conducted where noise is added artificially in increasing degrees. In the first test, Gaussian white noise is added and in the second test the proximity probe sampling rate is reduced. It is demonstrated that the proposed method recovers the noise-free tip deflections

more accurately than the other two methods for all levels of Gaussian noise addition. It is also found that the proposed method performs more accurately than the fixed voltage threshold method for all levels of sampling rate reduction. It is found that the proposed method is more accurate than the constant fraction crossing method in the initial levels of sampling rate reduction but becomes less accurate later on. This is ascribed to the apparent change in pulse shape caused by the reduction in sampling rate. Finally, a method is proposed whereby one can determine the scaling parameter, ρ , of the proposed method.

Some limitations of the proposed method are now discussed:

- **Constant shaft speed limitation.** The claims made in this article are only applicable to a rotor operating at a constant shaft speed. The proposed method has not yet been proven for transient speed cases. Transient speed cases may be more difficult to process because the pulse shape changes as the shaft speeds up. This is a problem that all triggering criteria have, not only the proposed method. Future investigations should assess whether the proposed method has the same advantages for transient shaft speeds.
- **Scaling parameter determination.** The scaling parameter, ρ, must be determined for every combination of probe and blade tip geometry. There is no single scaling parameter for all combinations of probes and blade tip geometries.
- **Blade resonance effect.** In this article, the blades are not experiencing resonance. The blades vibrate because of excitation from the ambient air. The presence of resonance would not affect the proposed method unless the shape of the pulse is changed by the resonance. It must be said that, if the shape of the pulse is affected by resonance, all triggering criteria will be affected. Studies need to be conducted to understand the effect resonance has on all triggering criteria.
- **Non-Gaussian forms of noise.** Gaussian noise is used in this article to demonstrate the proposed method's robustness to noise. There are other forms of noise in BTT. Examples being pulse shape changes due to increasing/decreasing temperature, axial shaft position shifts, pulse shape changes due to erosion etc. These sources of noise will affect the accuracies of all forms of triggering criteria. To the knowledge of the authors, no study has been conducted on how these sources of noise effect the accuracy of triggering criteria. Such a study would be very valuable for the BTT community.

The proposed method shows great promise to produce accurate tip deflections in the presence of noise or low sampling rates. This could lower the hardware cost of BTT systems, and consequently make its use more widespread. The proposed method has been open sourced and can be found at https://github.com/dawiediamond/pyphasetoa.

CRediT authorship contribution statement

D.H. Diamond: Conceptualization, Methodology, Software.

Declaration of Competing Interest

The authors declare that they have no known competing financial interests or personal relationships that could have appeared to influence the work reported in this paper.

Acknowledgements

Dawie Diamond has been supported by a Skye Foundation Scholarship in his PhD studies. The experimental setup used for the work reported in this article was partially funded by the Eskom Power Plant Engineering Institute (EPPEI). National Instruments South Africa is thanked for the use of their NI USB-6366 data acquisition system.

References

1. M. Zielinski, G. Ziller, Noncontact vibration measurements on compressor rotor blades, Measure. Sci. Technol. 11 (7) (2000) 847–856.
2. G. Dimitriadis, I.B. Carrington, J.R. Wright, J.E. Cooper, Blade-tip timing measurement of synchronous vibrations of rotating bladed assemblies, Mech.Syst. Signal Process. 16 (4) (2002) 599–622.
3. P. Beauseroy, R. Lengellé, Nonintrusive turbomachine blade vibration measurement system, Mech. Syst. Signal Process. 21 (4) (2007) 1717–1738, https://doi.org/10.1016/j.ymssp.2006.07.015. URL: http://linkinghub.elsevier.com/retrieve/pii/S0888327006001464.
4. D. Diamond, P.S. Heyns, A. Oberholster, Improved blade tip timing measurements during transient conditions using a state space model, Mech. Syst. Signal Process. 122 (2019) 555–579.
5. R. Szczepanik, E. Rokicki, R. Rzadkowski, L. Piechowski, Tip-Timing and Tip-Clearance for Measuring Rotor Turbine Blade Vibrations, Journal of Vibration Engineering & Technologies 2 (5).
6. A. Von Flotow, P. Tappard, Overview of Blade Vibration Monitoring Capabilities, 2011.
7. K. Grant, Experimental Testing of Tip-Timing Methods used for Blade Vibration Measurement in the Aero-Engine, Phd, Cranfield University, 2004..
8. N. Wadhwa, M. Rubinstein, F. Durand, W.T. Freeman, Phase-based video motion processing, ACM Trans. Graphics 32 (4) (2013) 10, URL http://dl.acm.org/citation.cfm?id=2461966.
9. J.G. Chen, N. Wadhwa, Y.-J. Cha, F. Durand, W.T. Freeman, O. Buyukozturk, Modal identification of simple structures with high-speed video using motion magnification, J. Sound Vib. 345 (2015) 58–71, https://doi.org/10.1016/j.jsv.2015.01.024, URL: http://linkinghub.elsevier.com/retrieve/pii/S0022460X1500070X.
10. A. Davis, M. Rubinstein, N. Wadhwa, G. Mysore, F. Durand, W. Freeman, The visual microphone: passive recovery of sound from video, ACM Trans. Graphics (TOG) 33 (4) (2014) 79–89.
11. D. Diamond, P. Heyns, A. Oberholster, Accuracy evaluation of sub-pixel structural vibration measurements through optical flow analysis of a video sequence, Measurement 95 (2017) 166–172.
12. B.R. Resor, M.W. Trethewey, K.P. Maynard, Compensation for encoder geometry and shaft speed variation in time interval torsional vibration measurement, J. Sound Vib. 286 (2005) 897–920, https://doi.org/10.1016/j.jsv.2004.10.044, URL: http://www.sciencedirect.com/science/article/pii/S0022460X0400882X.
13. K. Fyfe, E. Munck, Analysis of computed order tracking, Mech. Syst. Signal Process. 11 (1997) 187–205, URL http://www.sciencedirect.com/science/article/pii/S0888327096900564.
14. W.T. Freeman, E.H. Adelson, The design and use of steerable filters, IEEE Trans. Pattern Anal. Mach. Intell. 13 (9) (1991) 891–906.

15. T. Gautama, M.M. Van Hulle, A phase-based approach to the estimation of the optical flow field using spatial filtering, IEEE Trans. Neural Networks 13(5) (2002) 1–28, URL http://ieeexplore.ieee.org/xpls/abs_all.jsp?arnumber=1031944.
16. T. Zielinski, Instantaneous phase shift estimation methods, in: Quality Measurement: The Indispensable Bridge between Theory and Reality (No Measurements? No Science! Joint Conference-1996: IEEE Instrumentation and Measurement Technology Conference and IMEKO Tec, Vol. 1, IEEE, 1996, pp. 162–167.
17. D. Hale, An efficient method for computing local cross-correlations of multi-dimensional signals, CWP Report 656.
18. Z.S. Veličković, V.D. Pavlović, Complex analytic signals applied on time delay estimation, Facta universitatis-series: Phys. Chem. Technol. 6 (1) (2008) 11–27.
19. D.J. Fleet, D.J. Jepson, Computation of component image velocity from local phase information, Int. J. Comput. Vis. 5 (1) (1990) 77–104.
20. F.W. King, Hilbert transforms (volume 1), volume 124 of, Encyclopedia of Mathematics and its Applications.
21. G. Molnar, A. Milos, M. Vucic, Closed-form approximation of Hilbert transforms of Gaussian derivatives based on weighted polynomial fitting, in: 2018 41st International Convention on Information and Communication Technology, Electronics and Microelectronics (MIPRO), IEEE, 2018, pp. 0117–0121.
22. P. Procházka, F. Vaněkdamage, J. Phys. Conf. Ser. 305 (2011) 1–11, https://doi.org/10.1088/1742-6596/305/1/012116, URL: http://stacks.iop.org/1742-6596/305/i=1/a=012116?key=crossref.78d52140bb18e05748f8b3e84ce863df.
23. J. Gallego-Garrido, G. Dimitriadis, I.B. Carrington, J.R. Wright, A class of methods for the analysis of blade tip timing data from bladed assemblies undergoing simultaneous resonances-Part II: experimental validation, Int. J. Rotat. Mach. 2007 (2007) 1–10, https://doi.org/10.1155/2007/73624, URL: http://www.hindawi.com/journals/ijrm/2007/073624/abs/.
24. D. Di Maio, D.J. Ewins, Experimental measurements of out-of-plane vibrations of a simple blisk design using Blade Tip Timing and Scanning LDV measurement methods, Mech. Syst. Signal Process. 28 (2012) 517–527, https://doi.org/10.1016/j.ymssp.2011.09.018.
25. S. Heath, M. Imregun, An improved single-parameter tip-timing method for turbomachinery blade vibration measurements using optical laser probes. International journal of mechanical sciences 38 (10) (1996) 1047–1058